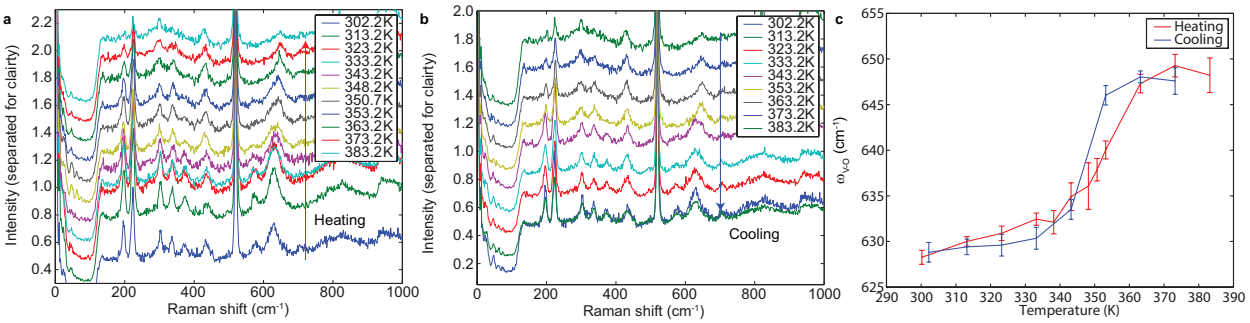


**Supplementary Figure** 1. **Thermal IMT hysteresis data on crystal #30.** Raman spectra of crystal #30 on heating (a) and cooling (b) through the thermal transition. Metallic stripes appear at 348 K and the microcrystal is fully metallic above 385 K. Extracted $\omega_{\mathrm{V-O}}$ peak position showing the evolution of the insulating phase through the T phase upon heating. At 363 K, the remaining insulating stripes transition to the M2 phase (see also [2]).

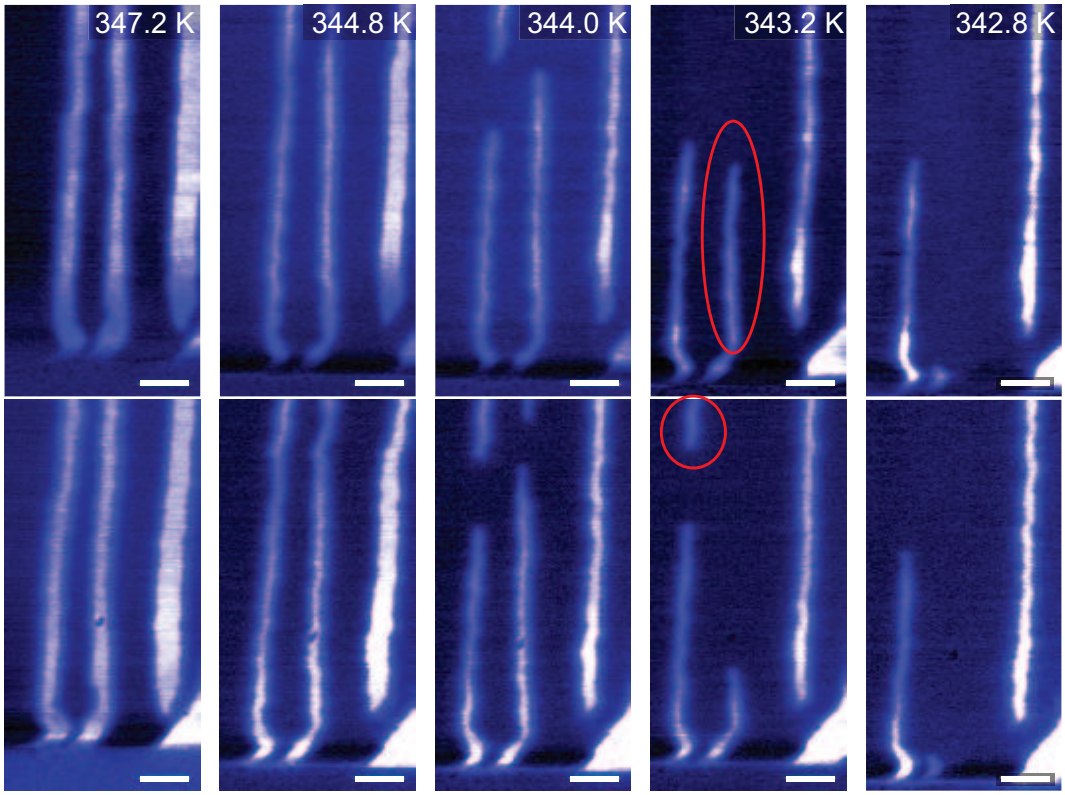


**Supplementary Figure** 2. **Variable domain pattern in the thermal IMT.** *s*-SNOM imaging during repeated cooling cycles showing irreproducible break-up pattern of metallic domains on a $VO_2$ microcrystal. Scale bars are 500 nm. Scans from the first cooling sequence (top row) and the second cooling cycle (bottom row, images at the same temperatures are stacked vertically) show a meandering pair of domains on the left that break around $T = 344.0$ K at nearly the same locations in the different cycles, but exhibit different domain patterns at $T = 343.2$ K (red circles) that cannot be explained by hysteresis effects since they begin and end with roughly the same domain pattern. This also may not be explained by difference in temperature since they are qualitatively different domain patterns that do not match a corresponding temperature in the other cycle.

| Crystal No. | Fluence (mJ $cm^{-2}$) | $\omega_{V-O}$ ($cm^{-1}$) | $\tau_f$ (fs) | $\tau_s$ (fs) | $a$ | Crystal size ($\mu$m) |
|---|---|---|---|---|---|---|
| 1 | 3.3 | 617.5 | 168 | 3580 | 0.02 | 33.6 |
| 2 | 5.3 | 631.4 | 70 | 2000 | 0.03 | 12.3 |
| 3 | 4.5 | 629.3 | 80 | 2050 | 0.1 | 5.5 |
| 4 | 3.3 | 630.2 | 92 | 2500 | 0.3 | 7.3 |
| 5 | 4.5 | 632.1 | 66 | 2000 | 0.1 | 10.4 |
| 6 | 4.5 | 632.5 | 71 | 2500 | 0.01 | 11.3 |
| 7 | 3.3 | 621.3 | 147 | 2000 | 0.3 | 4.9 |
| 8 | 3.0 | 627.2 | 125 | 2860 | 0.4 | 4.8 |
| | 3.7 | 627.2 | 128 | 2010 | 0.2 | 4.8 |
| 9 | 3.3 | 624.9 | 119 | 2000 | 0.3 | 6 |
| 10 | 3.3 | 618.7 | 118 | 2100 | 0.3 | 2.9 |
| 11 | 2.5 | 616.9 | 68 | 2000 | 0.1 | 3 |
| | 3.3 | 616.9 | 111 | 2590 | 0.2 | 3 |
| 12 | 2.4 | 626.2 | 55 | 2020 | 0.2 | 10 |
| 13 | 2.2 | 616.9 | 42 | 8620 | 3E-06 | 3 |
| | 2.4 | 616.9 | 77 | 5000 | 0.01 | 3 |
| | 2.5 | 616.9 | 92 | 2000 | 0.01 | 3 |
| | 2.8 | 616.9 | 92 | 2000 | 0.2 | 3 |
| 14 | 2.4 | 625.5 | 71 | 10000 | 0.01 | 9 |
| 15 | 2.3 | 626.3 | 76 | 9720 | 3E-05 | 9 |
| | 2.5 | 626.3 | 80 | 2010 | 0.05 | 9 |
| | 3.3 | 626.3 | 130 | 2010 | 0.2 | 9 |
| | 3.3 | 626.3 | 121 | 2760 | 0.4 | 9 |
| 16 | 2.4 | 617.1 | 97 | 9950 | 0.009 | 2.3 |
| | 2.6 | 617.1 | 84 | 9990 | 0.01 | 2.3 |
| 17 | 2.6 | 619.8 | 108 | 2000 | 0.2 | 4.8 |
| 18 | 3.6 | 625.5 | 97 | 2000 | 0.1 | 9 |
| | 3.6 | 625.5 | 83 | 3600 | 0.3 | 9 |
| 19 | 7.0 | 614.4 | 157 | 2000 | 0.2 | 6 |

| | | | | | | |
|---|---|---|---|---|---|---|
| 20 | 7.0 | 648.7 | 156 | 8250 | 0.002 | 6 |
| 21 | 5.3 | 632.2 | 42 | 9990 | 5E-07 | 11.5 |
| | 5.3 | 632.2 | 52 | 6840 | 2E-07 | 11.5 |
| 21(p) | 5.3 | 632.2 | 107 | 2000 | 0.05 | 11.5 |
| 22 | 8.2 | 640.2 | 71 | 10000 | 0.04 | 13 |
| 23 | 4.1 | 628.9 | 199 | 5860 | 0.01 | 2.5 |
| 24 | 4.1 | 641.5 | 119 | 2000 | 0.03 | 4.5 |
| 25 | 8.2 | 643.0 | 76 | 6710 | 5E-06 | 10.4 |
| 26 | 8.2 | 640.1 | 115 | 2010 | 0.2 | 5.6 |
| 27 | 8.2 | 642.7 | 42 | 6290 | 5E-07 | 7.5 |
| 28 | 8.2 | 642.7 | 107 | 2000 | 0.05 | 10 |
| 29 | 0.8 | 636 | | | | 7.2 |

**Supplementary Table** I: Fit parameters plotted in Figure 4 of main text. Measurement 21(p) was taken on crystal #21, with pump polarization perpendicular to the $c_R$-axis, while the other measurements were performed with pump parallel to the $c_R$-axis. Coherent phonon measurements were performed on crystal #29, at the specified fluence.

| Crystal No. | Fluence (mJ cm$^{-2}$) | $\omega_{\mathrm{V-O}}$ (cm$^{-1}$) | $\tau_f$ (fs) | $\tau_s$ (fs) | $a$ | Temperature (K) |
|---|---|---|---|---|---|---|
| 30 | 3.3 | 628.3 | 84.2 | 2000 | 0.2 | 297 |
| | 3.3 | 630.0 | 79.5 | 3150 | 0.45 | 313 |
| | 3.3 | 630.9 | 75.3 | 2010 | 0.15 | 323 |
| | 3.3 | 632.5 | 73.7 | 9090 | 1.4E-5 | 334 |
| | 3.3 | 634.9 | 62.1 | 9920 | 0.012 | 343 |
| | 3.3 | 640.0 | 7.6 | 5000 | 0.01 | 353 |

**Supplementary Table** II: Table of fit parameters shown in Figure 3c of main text.

## SUPPLEMENTARY NOTE 1. ADDITIONAL TEMPERATURE DEPENDENCE DATA FOR CRYSTAL #30

Here we present additional data on temperature dependence of microcrystal #30 regarding Figure 3c of the main text. Raman spectra are shown in Supplementary Figure 1a,b for heating and cooling cycles, respectively. Metallic domains appear at 348 K and the microcrystal is fully metallic above 385 K. Additionally, we observe the evolution of the insulating phase through the T phase with increasing temperature and the remaining insulating stripes transition to M2 at 363 K. This is indicated by the shift in the $\omega_{\mathrm{V-O}}$ peak position displayed in Supplementary Figure 1c. A 10 K hysteresis in the peak position is observed for the T-M2 transition. Supplementary Table 2 correlates the extracted $\omega_{\mathrm{V-O}}$ peak position with the ultrafast dynamics.

## SUPPLEMENTARY NOTE 2. FURTHER *s*-SNOM IMAGING

Here we provide further nanoscale images showing the irreproducible break up pattern of metallic puddles upon cooling through the thermal transition. Supplementary Figure 2 shows several thin metallic domain patterns during two repeated cooling cycles imaged with *s*-SNOM. Images taken at the same temperature are stacked vertically. The domains on the left break at roughly the same location at $T = 344.0$ K, but they show different domain patterns upon cooling to $T = 343.2$ K, as highlighted in the red circles. Since the domain patterns begin at 347.2 K and end at 342.8 K in qualitatively the same spatial arrangement, the different intermediate behavior cannot be explained by hysteresis effects. The large difference in the repeated scans at 343.2 K also cannot arise due to uncertainties in the temperature. Additionally, these metastable nanoscale metallic domains are observed to relax to a completely insulating state over temperature steps as small as $\Delta T = 0.1$ K, indicating their dynamic nature.

The irreproducibility illustrate the highly dynamical state of the microcrystals near the critical temperature $T_C$ which is extremely sensitive to spatial variations in the chemical potential and perturbations in the electronic structure. This highly dynamical state is in part a result of the free energy degeneracy of the rutile metallic and the two monoclinic insulating structures at $T_C$ [1]. As the crystal is cooled from $T_C$, the degeneracy is broken

and free energies begin to deviate, favoring the insulating phases. The insulating areas that first nucleate are observed to be in the M2 phase [2] due to the substrate-induced strain, which is predicted to have a structural free energy contribution closer to the rutile structure $\Delta H_{M1\to R} > \Delta H_{M2\to R}$ [3] and is therefore more sensitive to fine spatial variations in the free energy landscape.

## SUPPLEMENTARY REFERENCES


[1] Park, J. H. *et al.* Measurement of a solid-state triple point at the metal-insulator transition in $VO_2$. *Nature* **500**, 431–434 (2013).

[2] Jones, A. C., Berweger, S., Wei, J., Cobden, D. & Raschke, M. B. Nano-optical investigations of the metal-insulator phase behavior of individual $VO_2$ microcrystals. *Nano Lett.* **10**, 1574–1581 (2010).

[3] Pouget, J. P. *et al.* Dimerization of a linear Heisenberg chain in the insulating phases of $V_{1-x}Cr_xO_2$. *Phys. Rev. B* **10**, 1801 (1974).